Insight into the Mechanism of Inactivation and pH Sensitivity in Potassium Channels from Molecular Dynamics Simulations[†]

Phillip J. Stansfeld,[‡,§] Alessandro Grottesi,[||,⊥] Zara A. Sands,[||,@] Mark S. P. Sansom,[||] Peter Gedeck,[+] Martin Gosling,[+] Brian Cox,[+] Peter R. Stanfield,[#] John S. Mitcheson,[*,‡] and Michael J. Sutcliffe[*,▽]

Department of Cell Physiology and Pharmacology, University of Leicester, University Road, Leicester LE1 7RH, U.K., Structural Bioinformatics and Computational Biochemistry Unit, Department of Biochemistry, University of Oxford, South Parks Road, Oxford OX1 3QU, U.K., Novartis Horsham Research Centre, Wimblehurst Road, Horsham, West Sussex RH12 5AB, U.K., Molecular Physiology Group, Department of Biological Sciences, University of Warwick, Coventry CV4 7AL, U.K., and Manchester Interdisciplinary Biocentre and School of Chemical Engineering and Analytical Science, University of Manchester, 131 Princess Street, Manchester M1 7DN, U.K.

Received March 20, 2008; Revised Manuscript Received May 21, 2008

ABSTRACT: Potassium (K^+) channels can regulate ionic conduction through their pore by a mechanism, involving the selectivity filter, known as C-type inactivation. This process is rapid in the hERG K^+ channel and is fundamental to its physiological role. Although mutations within hERG are known to remove this process, a structural basis for the inactivation mechanism has yet to be characterized. Using MD simulations based on homology modeling, we observe that the carbonyl of the filter aromatic, Phe627, forming the S_0 K^+ binding site, swiftly rotates away from the conduction axis in the wild-type channel. In contrast, in well-characterized non-inactivating mutant channels, this conformational change occurs less frequently. In the non-inactivating channels, interactions with a water molecule located behind the selectivity filter are critical to the enhanced stability of the conducting state. We observe comparable conformational changes in the acid sensitive TASK-1 channel and propose a common mechanism in these channels for regulating efflux of K^+ ions through the selectivity filter.

Ionic flux through K^+ channels is modulated by a number of mechanisms. The primary gate in potassium (K^+) channels is formed by an inner transmembrane helix bundle at the cytoplasmic membrane interface. Opening of this gate permits K^+ ions to permeate. However, ionic current may cease even while the cytoplasmic gate is open. This mechanism is broadly termed inactivation. In most voltage-gated K^+ (K_v) channels, the dominant form of inactivation is N-type, as the channel is blocked by the N-terminus of either the pore-forming or ancillary β subunits. The structural basis of N-type inactivation is well understood (*1*–*3*). These channels also possess a second mechanism, which is termed either slow or C-type inactivation. This process involves the selectivity filter of the channel (e.g., ref *4*; Figure 1) and is commonly considered as invoking a constriction that inhibits K^+ passage. In agreement, the structure of KcsA crystallized in a low concentration of K^+ [*5*; Protein Data Bank (PDB) entry 1K4D (*6*)] shows such a constriction. In spite of this, a structural basis for the mechanism of C-type inactivation has yet to be identified.

A recently determined crystal structure of the KcsA channel (PDB entry 2ATK) has revealed structural changes in the selectivity filter that may be associated with the voltage-dependent gating of the selectivity filter in KcsA. The mutant E71A crystal structure indicates that rotation of the carbonyl oxygens of Val76 and Tyr78 away from the conduction axis is possible, implicating these residues in a gating mechanism that is comparable to the C-type inactivation gating that occurs in K_v channels (*7*).

In contrast to other members of the K_v channel family, the human ether-a-go-go related gene (hERG)[1] K^+ channel does not undergo N-type inactivation, but its C-type inactivation mechanism is remarkably fast (*8, 9*), making it a good

[†] P.J.S. was supported by a MRC/Novartis CASE Studentship. Research in M.S.P.S.'s and P.R.S.'s laboratories is supported by the Wellcome Trust; research in J.S.M.'s laboratory is supported by the MRC and the British Heart Foundation; research in M.J.S.'s laboratory is supported by the BBSRC, MRC and EPSRC.

* To whom correspondence should be addressed. M.J.S.: Manchester Interdisciplinary Biocentre and School of Chemical Engineering and Analytical Science, University of Manchester, 131 Princess St., Manchester M1 7DN, U.K.; telephone, +44 (0)161 306 2672; fax, +44 (0)161 306 5201; e-mail, mike.sutcliffe@manchester.ac.uk. J.S.M.: Department of Cell Physiology and Pharmacology, University of Leicester, University Road, Leicester LE1 7RH, U.K.; telephone, +44 (0)116 229 7133; fax, +44 (0)116 252 5045; e-mail, jm109@leicester.ac.uk.

[‡] University of Leicester.

[§] Present address: Structural Bioinformatics and Computational Biochemistry Unit, Department of Biochemistry, University of Oxford, South Parks Road, Oxford OX1 3QU, U.K.

[||] University of Oxford.

[⊥] Present address: CASPUR Consorzio Interuniversitario per le Applicazioni del Supercalcolo per Universita′ e Ricerca, Via dei Tizii, 6b, 00185 Roma, Italy.

[@] Present address: AstraZeneca R&D, Ion Channel Chemistry, Södertälje SE-151 85, Sweden.

[+] Novartis Horsham Research Centre.

[#] University of Warwick.

[▽] University of Manchester.

[1] Abbreviations: hERG, human ether-a-go-go related gene; TASK-1, TWIK-related acid-sensitive 1; SID, self-interacting domain; TEA, tetraethylammonium; MD, molecular dynamics.

10.1021/bi800475j CCC: $40.75
Published on Web 06/18/2008

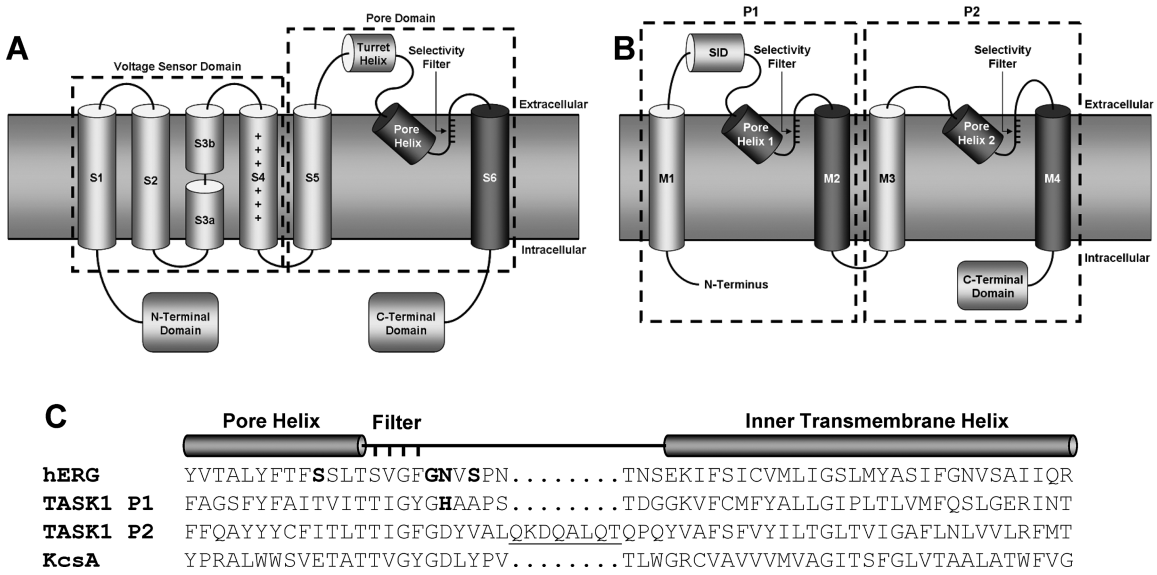

FIGURE 1: Topologies and sequence alignment of hERG and TASK-1. Schematic diagrams of (A) hERG and (B) TASK-1 illustrating the transmembrane domain topology of an individual subunit. The region of hERG and TASK-1 modeled in this study is shown in black. (C) Sequence alignment of both hERG and TASK-1 with KcsA. A single subunit of TASK-1 constitutes two pore-lining sequences (P1 and P2). The sequence of TASK-1 not modeled is underlined. The residues that are important to this study are shown in bold.

model system for the study of this process. The hERG channel constitutes the pore-forming α subunit of a voltage-gated K^+ current (I_{Kr}) that has an essential role in normal cardiac repolarization (*10*). Although the hERG channel is activated upon depolarization, the channel rapidly shifts into an inactivated state, with a time constant of 12 ms at −20 mV, to prevent K^+ efflux (*9, 10*). This enables the long plateau that is characteristic of a cardiac action potential. As the cell slowly repolarizes, the hERG channel leaves its inactivated state and re-enters the open state, thereby increasing the rate of cardiac repolarization. Inherited mutations of hERG result in abnormal repolarization of the action potential. Most increase the interval between the Q and T wave of the electrocardiogram (ECG), causing type 2 long QT syndrome (LQTS), which carries an increased risk of arrhythmias and sudden death (*11, 12*).

Inactivation can be disrupted by several mutations in and around the selectivity filter. In particular, a number of functionally well-characterized mutations are known to completely abolish inactivation in hERG. These mutations include S620T in the pore helix (*13*), a LQT2 mutant N629D, which follows directly after the GxG triplet in the selectivity filter (*14*), and G628C/S631C; Ser631 is also found at the extracellular aspect of the selectivity filter (*9*). The locations of these residues are consistent with those regulating C-type inactivation in other K_v channels, e.g., Shaker (*15*). Although these mutations have revealed the region of the channel that is involved in inactivation in hERG, a mechanistic and structural understanding of this fundamental process has remained elusive.

TASK-1 is a member of the tandem pore K^+ (K_{2P}) channel family (*16*), the members of which are responsible for maintaining the resting membrane potential by permitting conduction of K^+. The mechanism of inactivation in TASK-1 is regulated by extracellular pH, with the channel closing in response to acidification (*17*). This pH sensitivity is believed to be controlled by a histidine (His98) (*18–20*), which directly follows the signature sequence of the selectivity filter at the position analogous to that of Asn629 of hERG. Protonation of His98 in TASK-1 is likely to have an impact on the structure of the selectivity filter, transferring the channel into a nonconducting state.

To improve our understanding of the inactivation process, we investigated using molecular dynamics (MD) simulations the dynamics of homology models of the wild-type hERG conduction pore and three previously characterized non-inactivating mutants, S620T (*21*), N629D (*14*), and G628C/S631C (*9*). The roles of other residues in and around the selectivity filter are also explored. In addition to this, we investigate the effect of the protonation state of His98 side chain in TASK-1 on the stability of the selectivity filter. The locations of all residues involved are shown in Figure 2.

EXPERIMENTAL PROCEDURES

Homology Modeling. Modeller 7v7 (*22*) was used to create homology models of hERG [SWISS-PROT (*23*) entry Q12809] and TASK-1 (O35111) from the KcsA crystal structure [PDB entry 1K4C (*5*)] using the sequence alignment described in ref *24*. For hERG, four individual subunits were modeled, incorporating the region from Tyr611 at the N-terminal end of the pore helix to Arg666, at the C-terminal end of the S6 transmembrane helix (see Figure 1); 4-fold symmetry restraints were applied to the tetramer. These models of hERG do not include the S5-P linker (turret) (Figure 1A).

All hERG mutant channels, except G628C/S631C, were created from the wild-type hERG model, using the mutagenesis function in the Pymol molecular graphics system (*25*). G628C/S631C was created from the wild-type model, using Modeller 7v7 (*22*), with an intrasubunit disulfide bridge restraint applied between the two introduced cysteine residues and all other side chain conformations kept as in the wild type; 4-fold symmetry restraints were again applied. The degree of sequence identity between KcsA and hERG for the region modeled is 21.4%.

For the tandem pore channel, TASK-1, the P1 and P2 segments of the subunit were treated as separate entities and

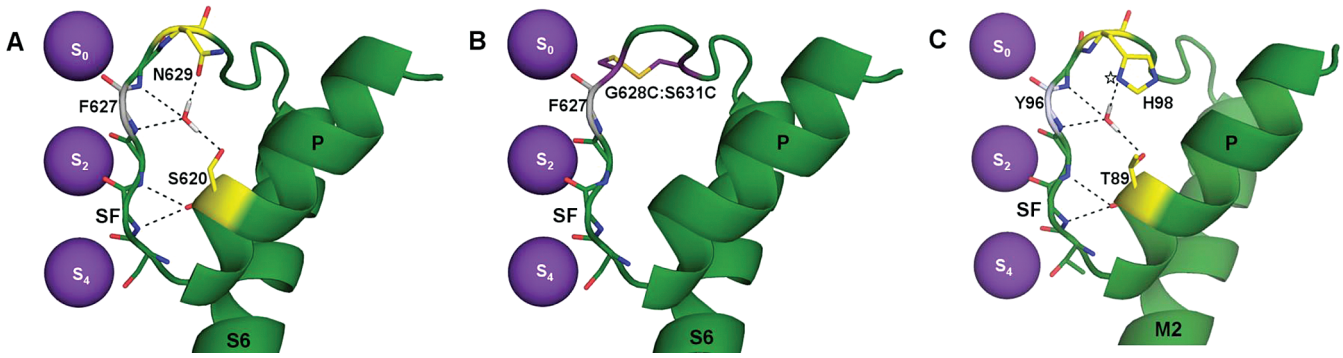

FIGURE 2: Behind the selectivity filter of hERG and TASK-1. Illustrations of the pore helix (P), selectivity filter (SF), and S6 transmembrane helix, prior to the beginning of the simulations. K^+ ions are positioned at sites S_0, S_2, and S_4 within the selectivity filter, and the water molecules at S_1 and S_3 are not shown. (A) Ser620 and Asn629 (both yellow) are predicted to form hydrogen bonds (dashed lines) with a water molecule behind the selectivity filter, which also interacts with the backbone amides of Phe627 (gray) and Gly628 (green). The carbonyl oxygen of Ser620 also forms hydrogen bonds with Val625 and Gly626. (B) Intrasubunit disulfide bridge formed between the inserted cysteine residues (purple) in the G628C/S631C hERG mutant. For clarity, the water molecule is not shown in this structure; it occupies the position shown in panel A, as do Ser620 and Asn629. (C) TASK-1 model, illustrating the interactions of the water molecule in this model with the backbone of Tyr96 (gray) and Gly97 (green), and the side chains of Thr89 and His98 (both yellow). The nitrogen atom of His98 that may be protonated is highlighted with a star.

modeled onto individual subunits of KcsA. P1 was modeled from Phe80 to Phe135, while P2 was modeled from Phe186 to Met251. Because of an extended postselectivity filter loop for P2, residues Gln210−Thr217 were omitted from the model (Figure 1C); 2-fold symmetry restraints were applied to the dimer. The degree of sequence identity between TASK-1 and KcsA is 19.6% for P1 and 21.4% for P2.

All models were compared to KcsA to verify that the modeling step had not significantly altered backbone and side chain conformations, with all residues located in the allowed regions of the Ramachandran plot. The hERG wild-type, S620T, and N629D models all have a Cα rmsd of 2.9 Å, with the G628C/S631C mutant having a rmsd of 2.8 Å and TASK models a rmsd of 3.2 Å compared to the KcsA crystal structure (PDB entry 1K4C).

MD Simulations. As performed previously (*26*), the homology models were incorporated into a POPC membrane bilayer, surrounded by solvent, using the protocol described in ref *27*. Voidoo and Flood were used to probe and add waters to the central cavity of the channel (*28*). K^+ ions were placed in the channel, using the crystallographic coordinates from KcsA, at K^+ sites S_0, S_2, S_4, and S_{cav}, with waters placed at S_1 and S_3 of the selectivity filter (*5, 29*). On the basis of the coordinates of the KcsA structure, a water molecule was also placed behind the backbone of the selectivity filter, in each of the four subunits. Cl^- ions were added at random within the solvent to neutralize the system. The periodic box surrounding the ∼17000-atom system had dimensions of ∼6 nm × 6 nm × 6.5 nm.

MD simulations were performed with Gromacs (version 3.2) (*30*) using the GROMOS96 43a1 force field (*31*). Simulations were performed using semi-isotropic pressure coupling with the Parrinello−Rahman barostat (*32*), while the temperature of the lipid, protein, and solvent (water and counterions) was separately coupled to an external bath kept at 300 K, using the Berendsen themostat (*33*). The SPC water model was used (*34*). The LINCS algorithm was used to constrain bond lengths (*35*). Long-range electrostatics up to 10 Å were modeled using the particle mesh Ewald (PME) method, while a cutoff of 10 Å was also used for van der Waals interactions. Gromacs was used to add hydrogen atoms to the models and to protonate His98.

Each system was initialized with a steepest descent energy minimization step, followed by 200 ps of restrained MD in which the non-hydrogen protein atoms and K^+ ions were restrained with a force constant of 1000. The system was then subjected to 10 ns of unrestrained MD, during which coordinates were saved every 10 ps for analysis.

pK_a Calculations. The pK_a values for all titratable amino acid side chains within the models were calculated using PROPKA (*36*). Amino acid protonation states were defined in an initialization step prior to the MD. The residues at the amino and carboxyl termini of the model were both considered as uncharged, as neither lie at the actual termini of the complete channel.

RESULTS AND DISCUSSION

The primary aim of this study was to investigate at the atomic level the process of selectivity filter inactivation gating that is proposed to occur in many K^+ channels. We have focused on the hERG channel, which undergoes rapid voltage-dependent inactivation, and compared its dynamics with those of TASK-1, which is sensitive to changes in extracellular pH. For both channels, we use known experimental data and seek to elucidate a structural basis for the mechanisms involved.

The gating in the hERG K^+ channel was studied by characterizing the MD of the wild-type channel model and investigating the effects of mutations that alter inactivation gating. The wild-type model of the hERG pore domain is a minimalistic representation of the complete channel, denoting the region of the channel that can be modeled with the most confidence. Thus, despite its likely role in inactivation, the S5-P linker (turret) of the channel is not included in the channel models. In the G628C/S631C model, the disulfide bridge links together a tight hairpin loop at the top of the selectivity filter; this does not significantly alter the shape of the extracellular mouth of the channel, despite the restraints imposed.

Although hERG and TASK-1 share a relatively low level of sequence homology with KcsA, there are now many crystal structures of K^+ channel proteins which, despite their differences in sequence [19−38% identical (Table 1 of the

Supporting Information)], have a very similar structure for the pore domain of the channel (*37–40*), particularly around the selectivity filter. Thus, KcsA is a suitable template structure for hERG and TASK-1 homology models (*18, 24*).

The gating process in the TASK-1 channel was assessed by comparing a MD simulation with an unprotonated His98 to a simulation with a protonated His98. In the models, the additional hydrogen atom on the His98 residue extends into the small pocket behind the selectivity filter.

Over the 10 ns period of the simulations, all six models are relatively stable with a typical Cα rmsd of ~2.8 Å, which is comparable to results of previous studies of this nature (e.g., ref *41*).

K^+ Ion Coordination in the Selectivity Filter. K^+ ions are coordinated in the selectivity filter of K^+ channels by a set of carbonyl oxygens, which mimic the first hydration shell of the ion and enable K^+ ion selectivity while retaining a throughput close to the rate of diffusion (*42*). There are four fully dehydrated K^+ ion sites, labeled S_1-S_4 from the extracellular side, although the last of which, S_4, is partly formed by a hydroxyl side chain of either a threonine or serine. A partially dehydrated site is also found at the outer mouth of the channel, with an ion interacting with the outermost carbonyl oxygens of the aromatic residue; this site is termed S_0 (*5*).

Because of electrostatic repulsion, ions are located at alternate sites within the selectivity filter, and thus, all systems were equilibrated with K^+ ions at sites S_0, S_2, and S_4 (*5*). In most of the simulations, the K^+ ions are well coordinated in the S_2 and S_4 sites for the entire simulation (Figure 3). In addition, in other simulations that started with K^+ ions in sites S_1 and S_3, the ions moved rapidly to S_2 and S_4 (data not shown). The only variant in this set is the G628C/S631C hERG mutant, in which the S_1-S_3 configuration is also adopted (Figure 3D). This is likely due to the enhanced stability of the S_1 coordination site in this mutant model (discussed below).

Comparison of the position of the K^+ ion at S_0 between the wild-type and mutant hERG models revealed differences in the ability of the channels to coordinate the ion at the extracellular mouth of the pore (Figure 3). In the wild-type hERG simulation, the K^+ ion is rapidly destabilized from the S_0 site, while in the non-inactivating mutants, S620T and N629D, the K^+ ion retains its coordination. The S_0 site is initially retained in the G628C/S631C simulation; however, the changes in K^+ ion coordination, in the selectivity filter, from S_2-S_4 to S_1-S_3 causes an electrostatic repulsion of the S_0 ion from its site, toward the S_{ext} site, in accord with the KcsA crystal structure (PDB entry 1K4C) (*5*). The instability of the S_0 ion in two wild-type structures of hERG was also observed in another recent molecular dynamics study (*43*). In this study, to overcome this, the authors were required to pull the S_0 ion toward the selectivity filter to retain coordination. In the wild-type simulation, both the K^+ ion at the S_0 site and the electronegative surface are less readily retained (Figure 4). In another recent study, the turret was also suggested to be involved in decreasing the electronegativity of the outer mouth of the channel and thus preventing K^+ permeation (*44*).

The Selectivity Filter Aromatic Phe627 Acts as a Gate in hERG. At S_0, a K^+ ion is partially dehydrated and primarily forms contacts with the backbone carbonyl oxygens of the aromatic residue, Phe627, at the center of the GFG triplet in hERG (*5*). In the wild-type hERG simulation, the peptide bond between the aromatic and the second glycine is mobile and the backbone of the Phe627 rapidly moves from an α-helical to a *β*-strand conformation in the Ramachandran plot, rotating the carbonyl oxygen away from the conduction axis (Figures 3A and 5). An enhanced instability of the outer mouth of the selectivity filter, focused on Phe627, was also observed by Massetti et al. in their models (*43*).

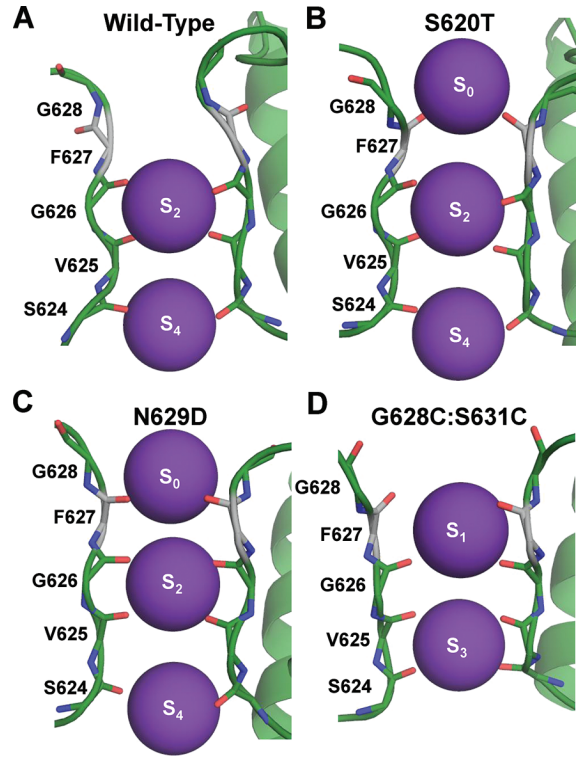

FIGURE 3: K^+ ion coordination within the selectivity filter. Snapshots of the selectivity filter in the hERG models after 1 ns of MD simulations. In each case, only two subunits are shown. (A) In the wild type, the carbonyl oxygens of the Phe627 residues have rotated away from the conduction axis, and the S_0 K^+ ion has vacated its coordination site. In (B) S620T and (C) N629D, the S_0 K^+ ion site is retained in both simulations, with ions preserved at S_2 and S_4 sites. (D) In the G628C/S631C simulation, the ions in the filter have moved from an S_2-S_4 to an S_1-S_3 configuration, illustrating that the carbonyl oxygen of Phe627 does not rotate away and therefore the S_1 coordination site is retained in this mutant. Because of the electrostatic repulsion between ions, the S_0 K^+ ion moves to the S_{ext} site (not shown). The disulfide bonds also retain the position of the carbonyl oxygens of Phe627, thus enhancing the electronegativity of the outer mouth of the channel and making K^+ ion passage more favorable.

This conformational change removes both the S_0 and S_1 K^+ ion coordination sites, making K^+ ion passage less favorable and thus impeding conduction. We propose that this conformational change underlies inactivation gating. Notably, this prevents the S_1-S_3 configuration of ions in the selectivity filter and explains why ions in the wild-type hERG model favor the S_2-S_4 sites. It is also notable that the wild-type simulation of hERG shows constriction about the S_0 site, constraining the extracellular portion of the selectivity filter, enhancing the hydrophobic barrier for K^+ passage.

A similar rotated conformation for the selectivity filter aromatic residue was observed at this position in the recently

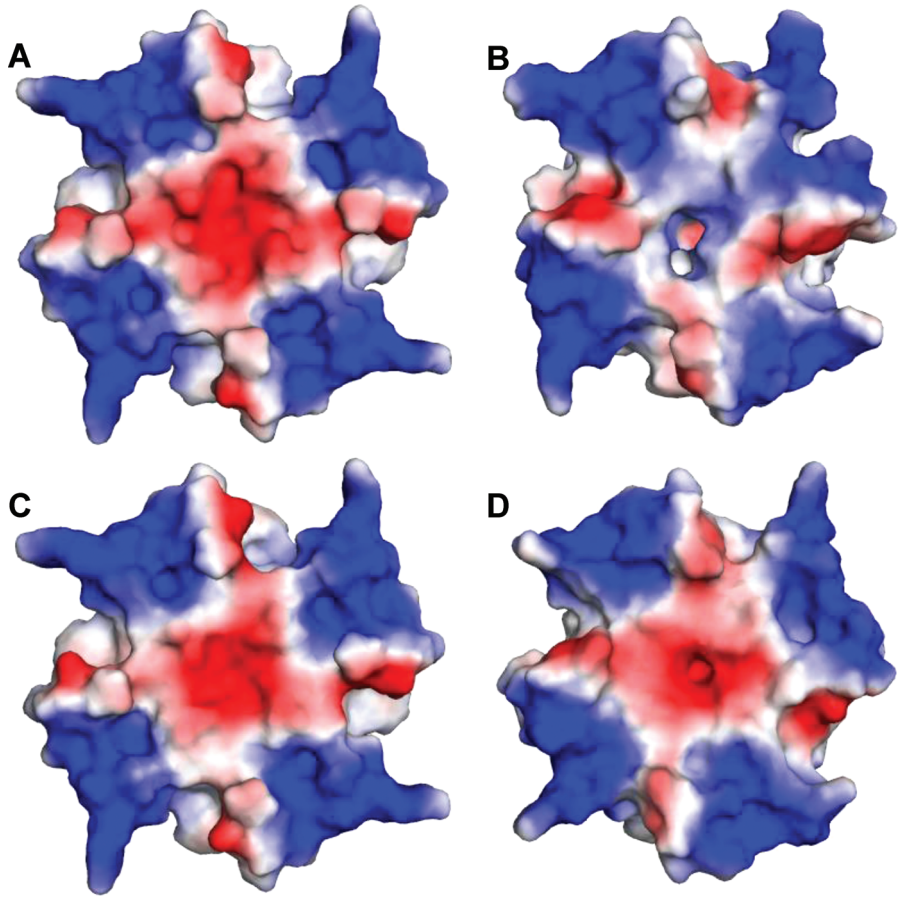

FIGURE 4: Electrostatic surfaces of the extracellular face of hERG. The negative electrostatic surface (red) at the channel mouth acts to stabilize the S_0 K^+ ion. Electrostatic surface maps are shown for the wild-type model after (A) 200 ps of restrained simulation and (B) 1 ns of full simulation and for the G629C/S631C mutant after (C) 200 ps of restrained simulation and (D) 1 ns of full simulation. While the negative electrostatic surface at the channel outer mouth of the wild-type simulation is lost in panel B, it is retained in the G629C/S631C simulations (D). This stabilizes the S_0 K^+ ion near the extracellular mouth of the channel, close to the S_{ext} site observed in the KcsA crystal structure (PDB entry 1K4C). The electrostatic surface maps were calculated using Pymol (*25*).

determined crystal structure of an E71A mutant (E71A "flipped") KcsA channel (PDB entry 2ATK) (*45*) and has been proposed for the peptide bond preceding the GxG triplet in other K^+ channels (*46*). It should be noted that although the E71A KcsA mutant has a high open probability (P_o), the flipped E71A crystal structure contains little or no density at the S_0 and S_{ext} ion binding sites (*45*). This apparent paradox,- in which the selectivity filter structure does not appear to reflect the conducting state, could be explained by the E71A mutant structure being crystallized with the selectivity filter stabilized by Fab fragments that bind to the extracellular mouth of the channel. Despite this uncertainty, recent functional studies of KcsA mutants (*45*), consistent with our findings for hERG mutants, indicate the importance of charged and polar residues behind the selectivity filter for channel conduction.

A high concentration of extracellular K^+ alters inactivation gating in hERG (*10*) and moderates pH sensitivity in TASK-1 (*17*), tending to stabilize the channel in an open, conducting state. In the simulations, the outermost K^+ ion, at the S_0 site, interacts with the carbonyl oxygen of the aromatic to reduce the rotation of the selectivity filter backbone, with the motion of the K^+ ion away from the S_0 site preceding the reorientation of the peptide bond. This is consistent with the effects of extracellular K^+ on increasing the open probability of both hERG and TASK-1 channels. Tetraethylammonium (TEA) is known to have a similar effect on C-type inactivation and is suggested to bind close to the S_0 site, based on mutational data and a KcsA crystal structure (PDB entry 2BOC) (*47, 48*). We suggest that the positive charge of both K^+ and TEA is able to stabilize the carbonyl oxygens at the extracellular mouth of the selectivity filter and therefore maintain the channel in the conducting conformation.

Water Molecules behind the Selectivity Filter Stabilize the Pore. Water molecules were first identified behind the selectivity filter in two crystal structures of KcsA, one of which was resolved at high K^+ concentrations (PDB entry 1K4C) and contained only one water molecule behind the filter of each individual subunit and the second of which was crystallized at low K^+ concentrations (PDB entry 1K4D) and contained two additional water molecules behind the filter (*5*).

In all hERG models, a small cavity is evident behind the selectivity filter, in the vicinity of the water molecule that was observed in the high-K^+ concentration KcsA (PDB entry 1K4C) crystal structure (*5*). Prior to the beginning of all simulations, one water molecule was positioned at this site, in all four subunits. Upon equilibration of the system, the water molecule relaxes so that it accepts two hydrogen bonds from the backbone amides of Phe627 and Gly628 in the selectivity filter, while donating its two hydrogen atoms to

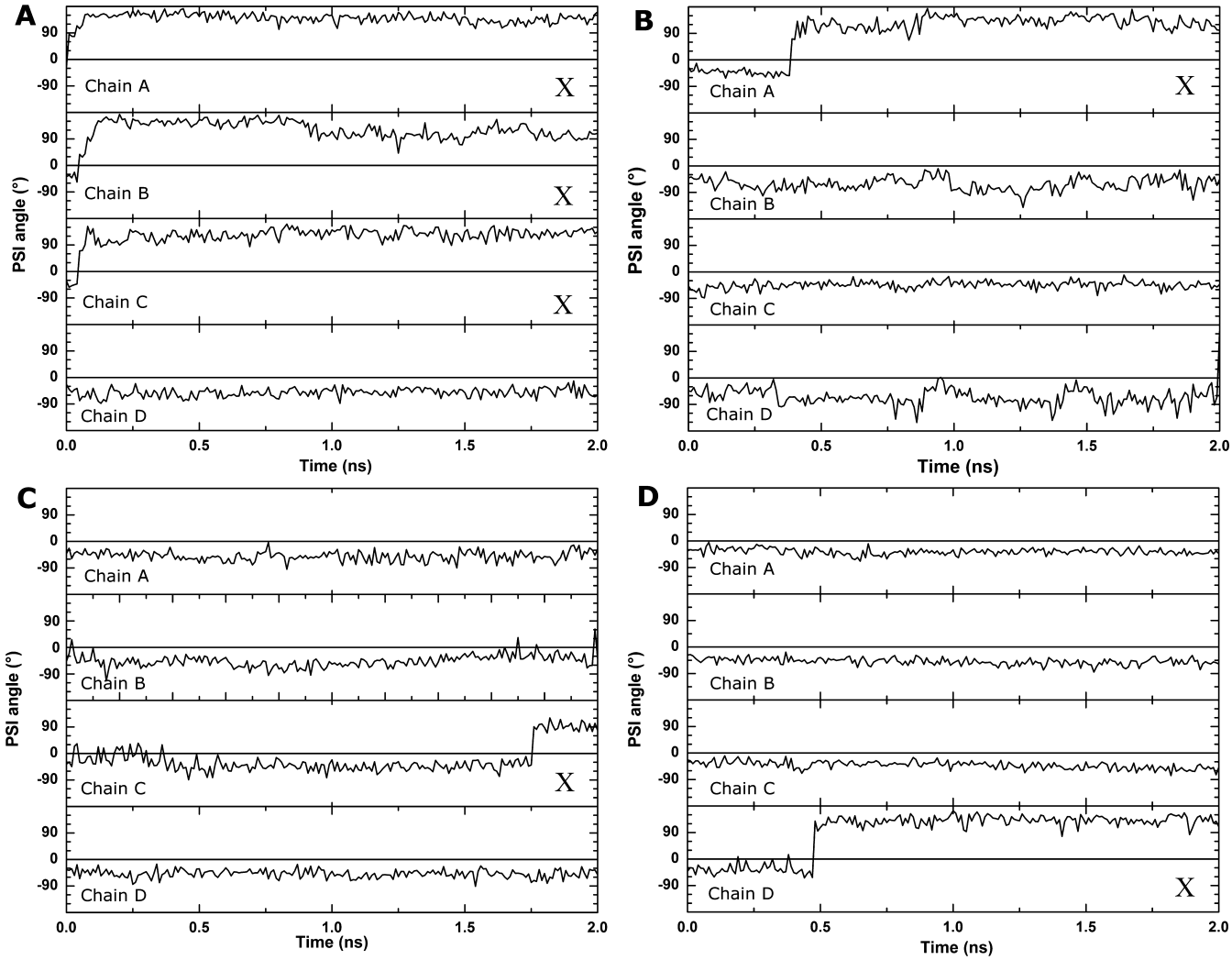

FIGURE 5: Rotation of the hERG Phe627 carbonyl oxygen. The conformation of the Phe627 carbonyl oxygen may be measured by the ψ angle of the F627−G628 peptide bond. When the bond is facing the conduction axis, the angle is approximately −50°, while an angle of approximately +100° indicates that the carbonyl has rotated away. The carbonyls that have rotated away are marked with X's. (A) Phe627 is very unstable in the wild-type simulation, resulting in a rapid rotation of three carbonyl oxygens away from the conduction axis. This event does not occur as frequently in the (B) N629D, (C) S620T, and (D) G629C/S631C simulations, with only one carbonyl oxygen shown to rotate away in the first 2 ns.

form hydrogen bonds with the side chains of Ser620 and Asn629 (Figure 2A).

These interactions are indicative of the importance of the water molecules as they act to stabilize the selectivity filter in its conducting state. The interactions with the side chains are highly dependent on side chain conformation, and in wild-type hERG, the stability of the water is reduced by frequent alteration of the conformation seen for the side chains of both Ser620 and Asn629. These effects have an impact on the rigidity of the selectivity filter, as the water is not always in a suitable position or orientation to accept the two hydrogen bonds from the backbone amides, particularly that of the second glycine, which forms the rotating peptide bond with the filter aromatic (Figure 6A). Notably, the hydroxyl of Ser620 also frequently acts as a hydrogen bond donor to the water, thereby reducing the number of hydrogen bonds that the water can accept from the backbone amides in the selectivity filter.

In all three of the non-inactivating hERG mutants, which are minor changes to the overall structure of the channel, the stability and interactions of the water molecule appear to be crucial for the rigidity of the selectivity filter. The critical interactions and differences in the hERG mutant simulations are discussed below.

hERG S620T. The S620T mutation is a conservative substitution in the pore helix of the channel that abolishes inactivation in hERG. Interestingly, this residue is comparable to Glu71 in KcsA, a residue implicated in voltage-sensitive gating in KcsA (*45, 49*). Unlike Ser620, in the wild-type channel, the additional methyl of the S620T mutant appears to prevent the hydroxyl side chain from changing its conformation, and thus, the side chain oxygen atom is retained throughout the course of the simulation, in a position in which it can accept a hydrogen bond from the water, while donating its hydrogen to the carbonyl oxygen of either Tyr616 or Phe617 in the pore helix (Figure 6B). In contrast, the wild-type Ser620 retains this conformation for only 3.7% of the simulation. The position of the side chain methyl in a hydrophobic pocket may also have an additional impact by stabilizing the position of the aromatic side chain of Phe627 and in turn the backbone of the selectivity filter (Figure 6C).

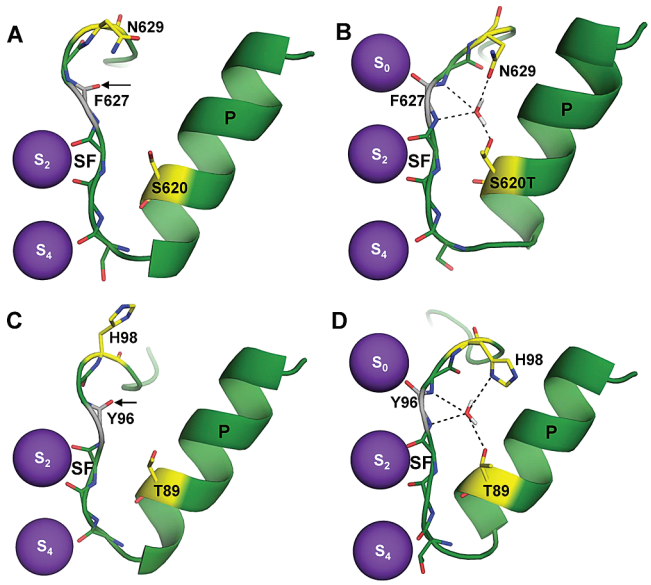

FIGURE 6: Comparison between hERG and TASK-1 simulations. Simulation snapshots after 1 ns of MD, demonstrating the interactions of the water molecule behind a single subunit. (A) Wild-type and (B) S620T hERG simulations. (C) Protonated and (D) unprotonated His98 TASK-1 simulations. The wild-type hERG simulation is comparable to the TASK-1-protonated His98 simulation, while the mutant hERG simulations, as exemplified by S620T, are similar to the simulation of TASK-1 when His98 is unprotonated.

hERG N629D. The N629D mutation is a disease-associated mutant that has also been previously shown in functional studies to be non-inactivating (*14*). In the simulation, it appears that a combination of the ring of negative charge at the extracellular mouth (as predicted by our pK_a calculations) and the additional hydrogen bond acceptor of the aspartate side chain [the more standard residue at this position in K^+ channels (*50*)] helps to stabilize the S_0 K^+ site (Figure 6B). In a number of the subunits, the distance between N629D and Lys638 is suitable for salt bridge formation, as predicted between equivalent residues Asp80 and Arg89 in KcsA (*37, 51*). This potential salt bridge also aids in the stabilization of the outer mouth of the pore.

hERG G628C/S631C. The G628C/S631C mutant hERG channel was one of the first mutated channels to be identified as non-inactivating, enabling the characterization of the C-type inactivation process in hERG (*9*). Although the interactions with the water molecule are still favorable in this mutant, the disulfide bridge formed between the two inserted cysteine residues is the more important factor. In the model and simulations the disulfide bridge rigidifies the extracellular mouth of the selectivity filter (Figure 6D) by linking a tight hairpin loop that is present in the KcsA crystal structure. This in turn stabilizes the side chain of Asn629 and the backbone carbonyl of Val630 so that either is in a suitable position to form hydrogen bonds with the water molecule. In turn, the water molecule interacts with the hydroxyl of Ser620 and the backbone amide of Gly628. The disulfide bond also restrains the carbonyl of G628C, thereby preserving the electronegativity of the channel outer mouth (Figure 4). This permits the retention of a K^+ ion in and around the S_0 and the more external S_{ext} sites throughout the duration of the 10 ns simulation. This electronegative surface is likely to be important for drawing the K^+ ions out of the selectivity filter as they move toward the extracellular side.

TASK-1. The water molecules behind the selectivity filter also appear to be highly important in the TASK-1 channel. In this instance, the water molecule interacts with the backbone amides of Tyr96 and Gly97, and the side chains of Thr89 and the putative proton sensor His98 (Figure 2C). Prior to the MD simulations, it is apparent that the protonated form of His98 is no longer able to accept the hydrogen bond from the water molecule. This is confirmed in the simulations where the stability of the water molecule is disrupted. This leads to the loss of the water molecule, and as a result, the Tyr96−Gly97 peptide bond rotates to remove the carbonyl oxygens from the conduction axis (Figure 6C). Consequently, the S_0 K^+ ion is rapidly destabilized from its coordination site. This site is also influenced by the protonated His98 residue, which rotates up and creates an electropositive barrier to K^+ ions at the outer mouth of the channel (Figure 6C). In contrast, in the unprotonated His98 simulation, the interactions with the water molecule are retained and the conducting conformation of the selectivity filter is maintained (Figure 6D). The conformational change observed with His98 protonation is mechanistically similar to that observed in hERG, leading to the reorientation of the selectivity filter backbone and loss of conduction.

Limitations of the Study. First, it should be stressed that the time scale of 10 ns for the molecular dynamic simulations is too short to observe the inactivation process per se; onset of inactivation has time constants in the 2−16 ms range, at potentials between −20 and +40 mV (*9, 10, 52*). It is also worth mentioning that once the filter aromatic residue carbonyls rotate away, they do not return to the original conducting conformation, within the 10 ns time scale. Nevertheless, a similar time scale has proved sufficient for observation of the rotation of the carbonyls away in simulations of other K channels, e.g., KcsA (*46*) and KirBac1.1 (*41*) using both GROMOS96 and CHARMM force fields. Second, the simulations consider homology models of both hERG and TASK-1 that are a simplified portrayal of the complete channel, most importantly the turret, which mutagenesis experiments suggest has an important role in the inactivation process, is not modeled in hERG, as its structure in the complete channel is not known. The turret has been modeled in another recent study (*53*); however, despite the constraints imposed in these models, the turret structure remains highly hypothetical. We expect that the turret has a fundamental role in increasing the stability at the outer mouth of the channel, and thus, in this study we observe a faster transition into the inactivated state. It is notable that the experimental mutations are able to prevent inactivation even in the presence of the turret, and therefore, although important, the turret is seemingly not intrinsic to the inactivation mechanism. Ideally, it would be beneficial to incorporate this linker region and the outer helix into the simulations. In TASK-1, the domain equivalent to the turret is the self-interacting domain (SID); this domain is also not incorporated into the simulations discussed here. This segment is suggested to have a role to play in the pH sensitivity of other K_{2P} channels (*54*), and although this is contested (*55*), it would be advantageous to include the SID in future studies. Third, all simulations were performed with symmetric electrolyte on either side of the membrane and

without a transmembrane potential. In such a system, it is not possible to fully characterize how voltage controls the inactivation process in hERG. Finally, the simulations are based on a closed state model of the channel and suggest direct transitions from the closed to inactivated state. These are consistent with single-channel recordings (*56*) and Markov state models (*56, 57*) that indicate that hERG channel inactivation from closed states occurs with high probability, particularly at positive potentials. Thus, the closed state structure is a suitable starting point for simulations of inactivation gating. Simulations of open state structures may also provide insight into inactivation transitions from the open state. However, both MthK and KvAP crystal structures were determined at a lower resolution than the KcsA structure (PDB entry 1K4C), with MthK lacking side chains and KvAP potentially distorted by the non-native conformation of its voltage-sensor domain (*58*). Notwithstanding this, instabilities of the selectivity filter similar to those we describe were observed in a molecular dynamics study that used KvAP as a template (*43*).

Concluding Remarks. In this study, we have identified, using MD simulations coupled with homology modeling, a region of structural instability within the selectivity filter of two K^+ channels that may explain important aspects of inactivation gating. In particular, we identify a role for a water molecule, first observed in the KcsA crystal structure, in stabilizing the backbone of the selectivity filter. This water molecule appears to play a crucial role in forming a network of hydrogen bond interactions with the pore helix and selectivity filter that stabilize the backbone of the selectivity filter. In particular, this water molecule confers structural rigidity by bridging two residues previously associated with inactivation in hERG (Asn629 and Ser620) and pH sensitivity in TASK-1 (His98 and Thr89). This water molecule is more readily retained within the non-inactivating hERG mutants and unprotonated TASK-1 channels than in the wild-type hERG or protonated TASK-1 channels. The picture of inactivation and pH sensitivity emerging from this study is as follows. The interaction between the water molecule behind the selectivity filter and the backbone of the selectivity filter is not as stable in the wild-type hERG or protonated TASK-1 channels as in the mutant hERG or unprotonated TASK channels. This enables the carbonyl oxygen of the filter aromatic to rotate more readily away from the conduction axis, thus removing both S_0 and S_1 K^+ ion coordination sites and transferring the selectivity filter into a nonconducting state. Our models are in good agreement with experimental results. Our study proposes a common mechanism for regulating efflux of K^+ ion through the selectivity filter, which is likely to be shared by other members of the K^+ channel family. Furthermore, they provide structural insight into how mutations, including inherited and disease-causing ones, alter the conduction properties of hERG.

ACKNOWLEDGMENT

We thank members of both M.J.S. and J.S.M. laboratories for their helpful discussions.

SUPPORTING INFORMATION AVAILABLE

Percentage sequence identity and similarity for the pore domain of a selection of six nonidentical K^+ channel crystal structures are listed in Table 1. Despite the low degrees of sequence identity, the pore domains are generally quite similar in structure. Three of the structures are in the closed state (KcsA, KirBac1.1, and MLotiK), while the other three are in the open state (KvAP, MthK, and Kv1.2). This material is available free of charge via the Internet at http://pubs.acs.org.

REFERENCES

1. Antz, C., Geyer, M., Fakler, B., Schott, M. K., Guy, H. R., Frank, R., Ruppersberg, J. P., and Kalbitzer, H. R. (1997) NMR structure of inactivation gates from mammalian voltage-dependent potassium channels. *Nature 385*, 272–275.
2. Baker, K. A., Hilty, C., Peti, W., Prince, A., Pfaffinger, P. J., Wider, G., Wuthrich, K., and Choe, S. (2006) NMR-derived dynamic aspects of N-type inactivation of a Kv channel suggest a transient interaction with the T1 domain. *Biochemistry 45*, 1663–1672.
3. Gulbis, J. M., Zhou, M., Mann, S., and MacKinnon, R. (2000) Structure of the cytoplasmic β subunit-T1 assembly of voltage-dependent K^+ channels. *Science 289*, 123–127.
4. Kurata, H. T., and Fedida, D. (2006) A structural interpretation of voltage-gated potassium channel inactivation. *Prog. Biophys. Mol. Biol. 92*, 185–208.
5. Zhou, Y., Morais-Cabral, J. H., Kaufman, A., and MacKinnon, R. (2001) Chemistry of ion coordination and hydration revealed by a K^+ channel-Fab complex at 2.0 Å resolution. *Nature 414*, 43–48.
6. Berman, H. M., Westbrook, J., Feng, Z., Gilliland, G., Bhat, T. N., Weissig, H., Shindyalov, I. N., and Bourne, P. E. (2000) The Protein Data Bank. *Nucleic Acids Res. 28*, 235–242.
7. Cordero-Morales, J. F., Cuello, L. G., and Perozo, E. (2006) Voltage-dependent gating at the KcsA selectivity filter. *Nat. Struct. Mol. Biol. 13*, 319–322.
8. Trudeau, M. C., Warmke, J. W., Ganetzky, B., and Robertson, G. A. (1995) HERG, a human inward rectifier in the voltage-gated potassium channel family. *Science 269*, 92–95.
9. Smith, P. L., Baukrowitz, T., and Yellen, G. (1996) The inward rectification mechanism of the HERG cardiac potassium channel. *Nature 379*, 833–836.
10. Sanguinetti, M. C., Jiang, C., Curran, M. E., and Keating, M. T. (1995) A mechanistic link between an inherited and an acquired cardiac arrhythmia: HERG encodes the IKr potassium channel. *Cell 81*, 299–307.
11. Keating, M. T., and Sanguinetti, M. C. (2001) Molecular and cellular mechanisms of cardiac arrhythmias. *Cell 104*, 569–580.
12. Curran, M. E., Splawski, I., Timothy, K. W., Vincent, G. M., Green, E. D., and Keating, M. T. (1995) A molecular basis for cardiac arrhythmia: HERG mutations cause long QT syndrome. *Cell 80*, 795–803.
13. Suessbrich, H., Schonherr, R., Heinemann, S. H., Lang, F., and Busch, A. E. (1997) Specific block of cloned Herg channels by clofilium and its tertiary analog LY97241. *FEBS Lett. 414*, 435–438.
14. Lees-Miller, J. P., Duan, Y., Teng, G. Q., Thorstad, K., and Duff, H. J. (2000) Novel gain-of-function mechanism in K^+ channel-related long-QT syndrome: Altered gating and selectivity in the HERG1 N629D mutant. *Circ. Res. 86*, 507–513.
15. Lopez-Barneo, J., Hoshi, T., Heinemann, S. H., and Aldrich, R. W. (1993) Effects of external cations and mutations in the pore region on C-type inactivation of Shaker potassium channels. *Receptors Channels 1*, 61–71.
16. Goldstein, S. A., Bayliss, D. A., Kim, D., Lesage, F., Plant, L. D., and Rajan, S. (2005) International Union of Pharmacology. LV. Nomenclature and molecular relationships of two-P potassium channels. *Pharmacol. Rev. 57*, 527–540.
17. Duprat, F., Lesage, F., Fink, M., Reyes, R., Heurteaux, C., and Lazdunski, M. (1997) TASK, a human background K^+ channel to sense external pH variations near physiological pH. *EMBO J. 16*, 5464–5471.
18. Yuill, K. H., Stansfeld, P. J., Ashmole, I., Sutcliffe, M. J., and Stanfield, P. R. (2007) The selectivity, voltage-dependence and acid sensitivity of the tandem pore potassium channel TASK-1: Contributions of the pore domains. *Pfluegers Arch. 455*, 333–348.
19. Lopes, C. M., Zilberberg, N., and Goldstein, S. A. (2001) Block of Kcnk3 by protons. Evidence that 2-P-domain potassium channel subunits function as homodimers. *J. Biol. Chem. 276*, 24449–24452.

20. Morton, M. J., O'Connell, A. D., Sivaprasadarao, A., and Hunter, M. (2003) Determinants of pH sensing in the two-pore domain K^+ channels TASK-1 and -2. *Pfluegers Arch. 445*, 577–583.
21. Ficker, E., Jarolimek, W., Kiehn, J., Baumann, A., and Brown, A. M. (1998) Molecular determinants of dofetilide block of HERG K^+ channels. *Circ. Res. 82*, 386–395.
22. Sali, A., and Blundell, T. L. (1993) Comparative protein modelling by satisfaction of spatial restraints. *J. Mol. Biol. 234*, 779–815.
23. Boeckmann, B., Bairoch, A., Apweiler, R., Blatter, M. C., Estreicher, A., Gasteiger, E., Martin, M. J., Michoud, K., O'Donovan, C., Phan, I., Pilbout, S., and Schneider, M. (2003) The SWISS-PROT protein knowledgebase and its supplement TrEMBL in 2003. *Nucleic Acids Res. 31*, 365–370.
24. Stansfeld, P. J., Gedeck, P., Gosling, M., Cox, B., Mitcheson, J. S., and Sutcliffe, M. J. (2007) Drug block of the hERG potassium channel: Insight from modeling. *Proteins 68*, 568–580.
25. DeLano, W. L. (2002) The PyMOL Molecular Graphics System, DeLano Scientific, San Carlos, CA.
26. Hardman, R. M., Stansfeld, P. J., Dalibalta, S., Sutcliffe, M. J., and Mitcheson, J. S. (2007) Activation gating of hERG potassium channels: S6 glycines are not required as gating hinges. *J. Biol. Chem. 282*, 31972–31981.
27. Faraldo-Gomez, J. D., Smith, G. R., and Sansom, M. S. (2002) Setting up and optimization of membrane protein simulations. *Eur. Biophys. J. 31*, 217–227.
28. Kleywegt, G. J., and Jones, T. A. (1994) Detection, Delineation, Measurement and Display of Cavities in Macromolecular Structures. *Acta Crystallogr. D50*, 178–185.
29. Aqvist, J., and Luzhkov, V. (2000) Ion permeation mechanism of the potassium channel. *Nature 404*, 881–884.
30. van der Spoel, D., Lindahl, E., Hess, B., Groenhof, G., Mark, A. E., and Berendsen, H. J. (2005) GROMACS: Fast, flexible, and free. *J. Comput. Chem. 26*, 1701–1718.
31. Scott, W. R. P., Hunenberger, P. H., Tironi, I. G., Mark, A. E., Billeter, S. R., Fennen, J., Torda, A. E., Huber, T., Kruger, P., and van Gunsteren, W. F. (1999) The GROMOS biomolecular simulation program package. *J. Phys. Chem. A 103*, 3596–3607.
32. Parrinello, M., and Rahman, A. (1981) Polymorphic Transitions in Single-Crystals: A New Molecular-Dynamics Method. *J. Appl. Phys. 52*, 7182–7190.
33. Berendsen, H. J. C., Postma, J. P. M., Vangunsteren, W. F., Dinola, A., and Haak, J. R. (1984) Molecular Dynamics with Coupling to an External Bath. *J. Chem. Phys. 81*, 3684–3690.
34. Hermans, J., Berendsen, H. J. C., Vangunsteren, W. F., and Postma, J. P. M. (1984) A Consistent Empirical Potential for Water-Protein Interactions. *Biopolymers 23*, 1513–1518.
35. Hess, B., Bekker, H., Berendsen, H. J. C., and Fraaije, J. G. E. M. (1997) LINCS: A linear constraint solver for molecular simulations. *J. Comput. Chem. 18*, 1463–1472.
36. Li, H., Robertson, A. D., and Jensen, J. H. (2005) Very fast empirical prediction and rationalization of protein pK_a values. *Proteins 61*, 704–721.
37. Doyle, D. A., Morais Cabral, J., Pfuetzner, R. A., Kuo, A., Gulbis, J. M., Cohen, S. L., Chait, B. T., and MacKinnon, R. (1998) The structure of the potassium channel: Molecular basis of K^+ conduction and selectivity. *Science 280*, 69–77.
38. Kuo, A., Gulbis, J. M., Antcliff, J. F., Rahman, T., Lowe, E. D., Zimmer, J., Cuthbertson, J., Ashcroft, F. M., Ezaki, T., and Doyle, D. A. (2003) Crystal structure of the potassium channel KirBac1.1 in the closed state. *Science 300*, 1922–1926.
39. Nishida, M., Cadene, M., Chait, B. T., and MacKinnon, R. (2007) Crystal structure of a Kir3.1-prokaryotic Kir channel chimera. *EMBO J. 26*, 4005–4015.
40. Clayton, G. M., Altieri, S., Heginbotham, L., Unger, V. M., and Morais-Cabral, J. H. (2008) Structure of the transmembrane regions of a bacterial cyclic nucleotide-regulated channel. *Proc. Natl. Acad. Sci. U.S.A. 105*, 1511–1515.
41. Domene, C., Grottesi, A., and Sansom, M. S. P. (2004) Filter flexibility and distortion in a bacterial inward rectifier K^+ channel: Simulation studies of KirBac1.1. *Biophys. J. 87*, 256–267.
42. Noskov, S. Y., and Roux, B. (2006) Ion selectivity in potassium channels. *Biophys. Chem. 124*, 279–291.
43. Masetti, M., Cavalli, A., and Recanatini, M. (2008) Modeling the hERG potassium channel in a phospholipid bilayer: Molecular dynamics and drug docking studies. *J. Comput. Chem. 29*, 795–808.
44. Kutteh, R., Vandenberg, J. I., and Kuyucak, S. (2007) Molecular dynamics and continuum electrostatics studies of inactivation in the HERG potassium channel. *J. Phys. Chem. B 111*, 1090–1098.
45. Cordero-Morales, J. F., Cuello, L. G., Zhao, Y. X., Jogini, V., Cortes, D. M., Roux, B., and Perozo, E. (2006) Molecular determinants of gating at the potassium-channel selectivity filter. *Nat. Struct. Mol. Biol. 13*, 311–318.
46. Berneche, S., and Roux, B. (2005) A gate in the selectivity filter of potassium channels. *Structure 13*, 591–600.
47. Lenaeus, M. J., Vamvouka, M., Focia, P. J., and Gross, A. (2005) Structural basis of TEA blockade in a model potassium channel. *Nat. Struct. Mol. Biol. 12*, 454–459.
48. Pardo-Lopez, L., Zhang, M., Liu, J., Jiang, M., Possani, L. D., and Tseng, G. N. (2002) Mapping the binding site of a human ether-a-go-go-related gene-specific peptide toxin (ErgTx) to the channel's outer vestibule. *J. Biol. Chem. 277*, 16403–16411.
49. Cordero-Morales, J. F., Jogini, V., Lewis, A., Vasquez, V., Cortes, D. M., Roux, B., and Perozo, E. (2007) Molecular driving forces determining potassium channel slow inactivation. *Nat. Struct. Mol. Biol. 14*, 1062–1069.
50. Shealy, R. T., Murphy, A. D., Ramarathnam, R., Jakobsson, E., and Subramaniam, S. (2003) Sequence-function analysis of the K^+-selective family of ion channels using a comprehensive alignment and the KcsA channel structure. *Biophys. J. 84*, 2929–2942.
51. Guidoni, L., Torre, V., and Carloni, P. (1999) Potassium and sodium binding to the outer mouth of the K^+ channel. *Biochemistry 38*, 8599–8604.
52. Spector, P. S., Curran, M. E., Keating, M. T., and Sanguinetti, M. C. (1996) Class III antiarrhythmic drugs block HERG, a human cardiac delayed rectifier K^+ channel. Open-channel block by methanesulfonanilides. *Circ. Res. 78*, 499–503.
53. Tseng, G. N., Sonawane, K. D., Korolkova, Y. V., Zhang, M., Liu, J., Grishin, E. V., and Guy, H. R. (2007) Probing the outer mouth structure of the HERG channel with peptide toxin footprinting and molecular modeling. *Biophys. J. 92*, 3524–3540.
54. Morton, M. J., Abohamed, A., Sivaprasadarao, A., and Hunter, M. (2005) pH sensing in the two-pore domain K^+ channel, TASK2. *Proc. Natl. Acad. Sci. U.S.A. 102*, 16102–16106.
55. Niemeyer, M. I., Gonzalez-Nilo, F. D., Zuniga, L., Gonzalez, W., Cid, L. P., and Sepulveda, F. V. (2007) Neutralization of a single arginine residue gates open a two-pore domain, alkali-activated K^+ channel. *Proc. Natl. Acad. Sci. U.S.A. 104*, 666–671.
56. Kiehn, J., Lacerda, A. E., and Brown, A. M. (1999) Pathways of HERG inactivation. *Am. J. Physiol. 277*, 199–210.
57. Piper, D. R., Varghese, A., Sanguinetti, M. C., and Tristani-Firouzi, M. (2003) Gating currents associated with intramembrane charge displacement in HERG potassium channels. *Proc. Natl. Acad. Sci. U.S.A. 100*, 10534–10539.
58. Lee, S. Y., Lee, A., Chen, J., and MacKinnon, R. (2005) Structure of the KvAP voltage-dependent K^+ channel and its dependence on the lipid membrane. *Proc. Natl. Acad. Sci. U.S.A. 102*, 15441–15446.
59. Jiang, Y., Lee, A., Chen, J., Cadene, M., Chait, B. T., and MacKinnon, R. (2002) Crystal structure and mechanism of a calcium-gated potassium channel. *Nature 417*, 515–522.
60. Jiang, Y., Lee, A., Chen, J., Ruta, V., Cadene, M., Chait, B. T., and MacKinnon, R. (2003) X-ray structure of a voltage-dependent K^+ channel. *Nature 423*, 33–41.

BI800475J